Earth and Planetary Science Letters 357–358 (2012) 11–20

Contents lists available at SciVerse ScienceDirect

Earth and Planetary Science Letters

journal homepage: www.elsevier.com/locate/epsl

Electrical conductivity of enstatite as a function of water content: Implications for the electrical structure in the upper mantle

Baohua Zhang [a,b,*], Takashi Yoshino [a], Xiaoping Wu [b], Takuya Matsuzaki [a], Shuangming Shan [a,c], Tomoo Katsura [a,d]

[a] Institute for Study of the Earth's Interior, Okayama University, Misasa, Tottori-ken 682-0193, Japan
[b] School of Earth and Space Science, University of Science and Technology of China, Hefei 230026, PR China
[c] Laboratory for High Temperature & High Pressure Study of the Earth's Interior, Institute of Geochemistry, Chinese Academy of Sciences, Guiyang 550002, China
[d] Bayerisches Geoinstitut, Universität Bayreuth, D-95440 Bayreuth, Germany

ARTICLE INFO

Article history:
Received 8 April 2012
Received in revised form
1 August 2012
Accepted 17 September 2012
Editor: L. Stixrude
Available online 17 October 2012

Keywords:
electrical conductivity
orthopyroxene
water
upper mantle

ABSTRACT

The electrical conductivity of Ca-free aluminous enstatite with various water contents has been determined at a pressure of 3 GPa in a Kawai-type multi-anvil apparatus. Impedance spectroscopy was performed for both hydrogen-doped and -undoped samples in a frequency range from 0.1 Hz to 1 MHz to examine the effect of water on conductivity. Two conduction mechanisms were identified for hydrogen-undoped samples at temperature of 1000–1723 K and for hydrogen-doped samples at relatively lower temperature range of 500–900 K to minimize dehydration of samples. For the hydrogen-undoped samples, the activation enthalpy is around 1.9 eV at the higher temperatures range (>1300 K) suggesting that the dominant charge transfer mechanism is $Fe^{2+}-Fe^{3+}$ hopping (small polaron) conduction. For the hydrogen-doped samples measured below 900 K, the activation enthalpy decreases from 1.11 to 0.70 eV, and the conductivity values systematically increase with increasing water content, suggesting that proton conduction is the dominant conduction mechanism. Taking hopping conduction and water content dependence of activation enthalpy for proton conduction into account, all electrical conductivity data were fitted to the formula $\sigma=\sigma_{0h}\exp(-H_h/kT)+\sigma_{0p}C_w\exp[-(H_p^0-\alpha C_w^{1/3})/kT]$, where σ_0 is pre-exponential factor, C_w is the water content in weight percent, H is the activation enthalpy, H_p^0 is the activation enthalpy for proton conduction at very low water concentration, α is the geometrical factor, k is the Boltzmann constant, T is absolution temperature and subscripts h and p represent hopping and proton conductions, respectively. Using the present results, a laboratory-based conductivity-depth profile in the Earth's upper mantle has been constructed as a function of water content. Comparison of our model with the currently available geophysical observations beneath the Eastern Pacific Rise indicates that hydrous aluminous enstatite cannot account for the high conductivity anomaly at the top of the asthenosphere as well as hydrous olivine.

1. Introduction

Some conductivity models based on magnetotelluric surveys have indicated high-conductivity anomaly in the asthenosphere (Lizzarralde et al., 1995; Evans et al., 2005). Two hypotheses have been proposed to interpret high conductive values. One is olivine hydration (Karato, 1990; Evans et al., 2005) and another is partial melting (Shankland and Waff, 1977; Yoshino et al., 2006). To test the former hypothesis, several groups experimentally studied the effect of water on the electrical conductivity of olivine (Yoshino et al., 2006; Wang et al., 2006; Poe et al., 2010; Yang, 2012). Yoshino et al. (2006) showed that, although electrical conductivity of single crystal olivine increases with increasing water content, both relative contribution and anisotropy of proton conduction become weak at high temperature. Thus the high conductivity of the asthenosphere cannot be explained by hydrous olivine. In contrast, Wang et al. (2006) showed much higher conductivity and greater temperature dependence. They concluded that hydrous olivine should be responsible for the high conductivity of the asthenosphere. However, recent experimental studies (Yoshino et al., 2009; Poe et al., 2010; Yang, 2012) have verified the implausibility of proton conduction for explanation of the high conductivity of the asthenosphere.

Orthopyroxene is the second abundant constituent mineral of the shallow upper mantle. The partition coefficient of water of

* Corresponding author at: Institute for Study of the Earth's Interior, Okayama University, Misasa, Tottori-ken 682-0193, Japan. Tel.: +81 858 43 3758; fax: +81 858 43 2184.
E-mail addresses: zhangbh@cc.okayama-u.ac.jp, zhangbh@mail.ustc.edu.cn (B. Zhang).

0012-821X/$ - see front matter
http://dx.doi.org/10.1016/j.epsl.2012.09.020

aluminous enstatite to olivine is very high, $D_{H_2O}^{Opx/Ol} = 11.7$ (Grant et al., 2007), and the maximum water solubility in aluminous enstatite has the maximum values close to 1 wt% at low pressures (1.5 GPa) and temperatures (1073 K) (Mierdel et al., 2007). Thus, aluminous enstatite could be a more important host than olivine for water in the upper mantle. If the electrical conductivity of hydrous Al-bearing enstatite is significantly higher than that of hydrous olivine at constant bulk water content, it is expected that the high-conductivity anomaly in the asthenosphere (Lizzarralde et al., 1995; Evans et al., 2005) could be explained by the proton conduction of enstatite.

The earliest studies reported the electrical conductivity of orthopyroxene at ambient pressure (Duba et al., 1973; Huebner et al., 1979; Huebner and Dillenburg, 1995). Xu and Shankland (1999) reported the electrical conductivity of orthopyroxene at high pressures by implicitly assuming anhydrous conditions, attributing their conduction data to hopping conduction. The conductivity measurement on proton conduction of orthopyroxene was first reported by Dai and Karato (2009). Their results showed that water can greatly enhance the electrical conductivity of orthopyroxene. However, Dai and Karato (2009) did not determine the electrical conductivity of hydrous orthopyroxene as a function of water content. Recently, a similar study was conducted by Yang et al. (2012a), who measured the electrical conductivity of hydrous orthopyroxene with relatively lower water contents (only up to 375 ppm) at 573–1273 K and 0.6–1.2 GPa. The results for hopping and proton conductions by Yang et al. (2012a) largely disagree with the previous studies. Therefore, the effect of water on conductivity of orthopyroxene is still controversial.

In this study, we have measured the electrical conductivity of polycrystalline aluminous enstatite at 3 GPa as a function of water content by means of complex impedance spectroscopy in a Kawai-type multi-anvil apparatus. For the hydrogen-doped aluminous enstatite, conductivity measurements were performed at relatively low temperature of up to 900 K to minimize water loss from crystals. To separate the contribution of proton and small polaron conductions, conductivity of hydrogen-undoped enstatite was measured at up to 1723 K. We have constructed a laboratory-based conductivity model using our experimental data, and compared it with the geophysically observed conductivity-depth profiles to assess water content in the asthenosphere.

2. Experimental procedures

2.1. Sample preparation

Four different types of starting materials were used to synthesize the hydrogen-doped and -undoped orthopyroxene, which have the same Mg numbers [Mg/(Mg+Fe)=0.9] and various Al_2O_3 contents (Al-free, 3, 6 and 10 wt%). The starting materials were prepared from a mixture of MgO, Fe_2O_3, SiO_2 and Al_2O_3 oxides in the following procedure. The oxide powders were dried at 1273 K for 4 h, then mixed and ground in an agate mortar for 2 h. The glasses were synthesized from these mixtures by melting them under ambient pressure at 1873 K in air and quenching them into water. These glasses were finely ground and pressed into pellets. The pellets were heated in a furnace at 1473 K for 1 h with controlled oxygen partial pressure of log $fO_2 = -8.47$ [log atm], which is close to the QFM buffer, and then quenched into water.

Aluminous enstatite samples were sintered in an end-loaded piston-cylinder apparatus at 1 GPa and 1123–1473 K using 3/4 in. pressure assemblies, for durations up to 184 h. Hydrogen-doped (wet) aluminous enstatite samples were synthesized using mixtures of the aluminous enstatite and brucite powder as a water source (about 1 wt% H_2O). The mixtures were loaded into Mo capsule, and inserted the Mo capsule into a little larger Pt tube, then sealed by welding. The Mo capsule was also used to control fO_2 close to the Mo–MoO_2 buffer. The water content in the enstatite was obtained by changing the annealing conditions (Mierdel and Keppler, 2004; Mierdel et al., 2007) (for detail see Table S1 in the supplementary material). Finally, the samples were cooled to room temperature with a cooling rate of about 100 °C/min, which allowed us to obtain sintered enstatite without cracking due to thermal shock.

We also synthesized a sample without detectable amount of hydrogen to measure hopping conduction only. The starting material of Al-free enstatite powder was first dried at 473 K for one day in a vacuum furnace, one-end welded gold capsule was preheated on a 473 K heating plate, then the enstatite powder was put into gold capsule which was welded immediately. Finally, the sample was sintered at 6 GPa (see 5K1910 in Table S1 of the supplementary material) in a Kawai-type multi-anvil apparatus. Experimental conditions were summarized in Table S1 in the supplementary material.

2.2. Sample characterization

The sintered enstatite aggregate was cut into two pieces, one of which was doubly polished to thin section of less than 0.1 mm thickness. The thin section was used to characterize the sample before conductivity measurement. Phase identification was conducted by micro-focused X-ray diffraction. After the conductivity measurement, phases in the recovered samples were determined to be orthoenstatite, although small amounts of low-pressure ($P2_1/c$) clinoenstatite (Ulmer and Stalder, 2001) were observed in a few hydrogen-doped samples. The major element compositions were determined by an electron probe microanalyzer (EPMA) (JEOL JXA-8800) (see Table S2 in the supplementary material). The Mg numbers [Mg♯=Mg/(Mg+Fe_{total})] in hydrogen-doped aluminous enstatite sample with brucite are slightly higher than those of the samples without brucite (see Table S1 in the supplementary material). The Al concentrations and Mg♯ in aluminous enstatite are very close to those in the initial glass starting materials (Table S1 in the supplementary material). The sample textures were examined by scanning electron microscopy and the grain sizes were less than 20 μm.

The FT-IR spectra of the samples before and after conductivity experiments were obtained using Jasco Janssen MFT-2000 FT-IR

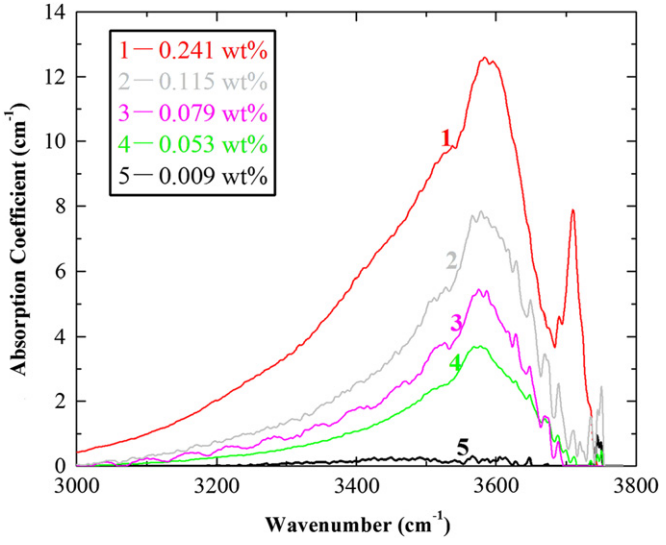

Fig. 1. Unpolarized FT-IR spectra of synthetic aluminous enstatite before the electrical conductivity measurements.

Table 1
Experimental results on the electrical conductivity of hydrous Al-bearing enstatite.

Run no.	Sample#	Water content (wt%)		T (K)	$\log\sigma_0$ (S/m)	H (eV)	Comments
		C^{α}_{OH}	C^{β}_{OH}				
1K1520	En0	<0.001	0.002(2)	1000–1300	1.09(20)	1.11(5)	Dry sample
				1300–1723	4.07(23)	1.90(7)	
5K1486	En1	0.079(15)	0.044(7)	500–900	0.86(18)	0.77(2)	Dehydration
5K1470	En4	0.053(5)	0.052(15)	600–800	0.49(10)	0.78(1)	
5K1476	En5	0.054(3)	0.053(5)	500–800	0.41(18)	0.76(2)	
1K1090	En7	n.d.	0.009(5)	600–900	0.99(41)	0.93(6)	
1K1101	En8	0.129(4)	0.053(7)	600–750	0.71(54)	0.72(7)	Dehydration
5K1492	En9	0.115(14)	0.057(12)	600–700	0.66(26)	0.73(3)	Dehydration
1K1095	En10	0.241(19)	0.235(4)	600–800	1.02(41)	0.70(6)	

All experiments were conducted at 3 GPa. Water content (in wt%), C^{α}_{OH} and C^{β}_{OH} are those of before and after conductivity measurements from FTIR spectroscopy. Errors are one standard deviation in parentheses.

spectrometer with unpolarized light. The water content in samples was calculated by the equation given by Paterson (1982). The spectra were obtained using less than 0.1 mm-thick sample in crack-free regions of $\sim 100\times 100\ \mu m^2$. At least five measurements were carried out at different areas for each sample. Representative FT-IR spectra of the samples with various amounts of water before the electrical conductivity measurement are shown in Fig. 1. The infrared spectra of aluminous enstatite aggregates display a strong absorption band around 3580–3590 cm^{-1} and weak absorptions around 3500–3520 cm^{-1} irrespective of the water content. These spectra are essentially the same as those reported for hydrous orthoenstatite (Bromiley and Bromiley, 2006; Mierdel et al., 2007; Yang et al., 2012b). Additionally, it has been claimed that the Paterson calibration for unpolarized FTIR spectra may underestimate water content in nominally anhydrous minerals (especially in olivine) by a factor of 3 (Mosenfelder et al., 2006) compared to the calibration of Bell et al. (2003). In this study, since the FT-IR measurements were carried out using the polycrystalline sample, the single crystal calibration methods (Bell et al., 2003) are not applicable to our samples and error of the water content calculated from the spectra through randomly oriented crystals would be smaller. The water contents in samples after conductivity measurement are shown in Table 1.

2.3. Electrical conductivity measurements

One half of the sintered aggregate was used for the conductivity measurement. Electrical conductivity measurements were carried out at 3 GPa in a Kawai-type multi-anvil apparatus. The cell design for the conductivity measurement is essentially the same as that in our previous study (Yoshino et al., 2006, 2009, 2010, 2012; Yoshino, 2010). A disc-shape sample was placed between two molybdenum electrodes. Mo serves also to buffer oxygen activity at the $Mo+O_2=MoO_2$ equilibrium during the measurement. This buffer is considered to be nearly identical to that of iron-wüstite ($Fe+1/2O_2=FeO$) (Xu et al., 1998). Prior to the experiment, the assembly was further dried overnight at 473 K in a vacuum furnace just before the conductivity measurement.

After compressing the sample assembly, we purged the adhesive water in the surrounding materials by pre-heating at 500 K for more than 2 h. While the sample was kept at this temperature, the sample resistance was frequently monitored. The resistance at the beginning of the first heating decreased due to release of absorbed water in the assembly. After the high insulation resistance ($\sim 10^8\ \Omega$) was obtained, conductivity measurements were started. Impedance spectroscopy was carried out using a Solartron 1260 impedance Gain-Phase Analyzer combined with a Solartron 1296 interface. Most data were obtained at frequencies ranging from 1 MHz to 1 or 0.1 Hz with 1.41 V applied voltage. According to previous studies on hydrous olivine (Yoshino et al., 2006, 2009), sample dehydration occurred at 1000 K during conductivity measurement. We found that hydrous enstatite starts dehydration at 900 K during heating. Therefore, a typical measurement was performed for hydrogen-doped enstatite samples by heating up to a maximum temperature 900 K. This upper temperature limit was chosen to minimize partial dehydration of sample at the maximum temperature of the measurement. In order to check the reproducibility of conductivity measurements, complex impedance spectra were obtained in several heating–cooling cycles. For each cycle, the maximum temperature was increased by 100 K step to identify the dehydration temperature. For hydrogen-undoped samples, conductivity was measured at temperatures up to 1723 K. During each cycle, temperature was changed by 50–100 K steps, and impedance spectra were obtained at each temperature step.

Impedance spectra showed only a symmetrical single arc over the temperature and frequency ranges investigated. An equivalent circuit consisting of a sample resistance and capacitance in parallel was used to fit the experimental data to determine sample resistance. Sample conductivity was calculated from the sample resistance and dimensions. Experimental errors are estimated to be less than 5%, which arise mainly from uncertainties in the dimensions of the sample and distortion of the impedance arcs.

3. Results

Fig. 2 shows the representative complex impedance spectra acquired for the hydrogen-doped and -undoped enstatite samples. All the complex impedance spectra of hydrogen-doped samples exhibit only one impedance arc in the investigated frequency range and at temperatures ranging from 600 to 800 K (Fig. 2a). Fig. 2b shows a series of complex impedance spectra for hydrogen-undoped sample at temperatures ranging from 1000 to 1500 K. The impedance arc at higher frequency range (1 MHz to 100 Hz) corresponds to the grain interior conduction, although a short tail appears at the end of the first impedance arc at frequencies lower than 100 Hz. The bulk sample resistance was determined using the high-frequency portion of the spectrum to fit the data.

The temperature dependence of conductivity (σ) can be expressed according to the Arrhenian relation:

$$\sigma=\sigma_0\exp\left(-\frac{H}{kT}\right) \quad (1)$$

where σ_0 is the pre-exponential factor, H is the activation enthalpy, k is the Boltzmann constant, and T is absolute temperature. Two typical

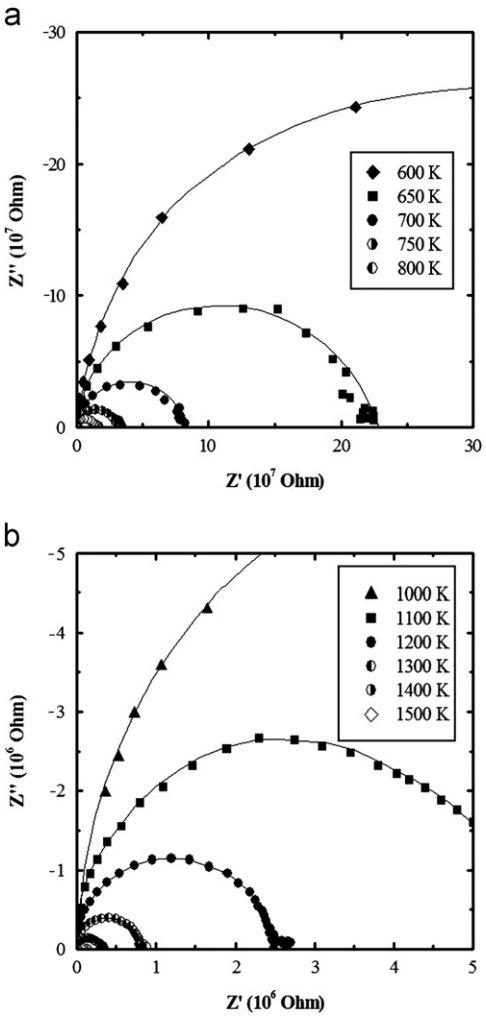

Fig. 2. Complex impedance spectra showing the semicircular pattern of the real (Z′) vs. imaginary (Z″) components of complex impedance at frequencies ranging from 1 MHz to 1 or 0.1 Hz at the temperatures indicated. (a) Impedance spectra of hydrogen-doped aluminous enstatite sample (run 5K1470) measured at temperatures ranging from 600 to 800 K. (b) Impedance spectra of hydrogen-undoped aluminous enstatite sample (run 1K1520) measured at temperatures ranging from 1000 to 1500 K.

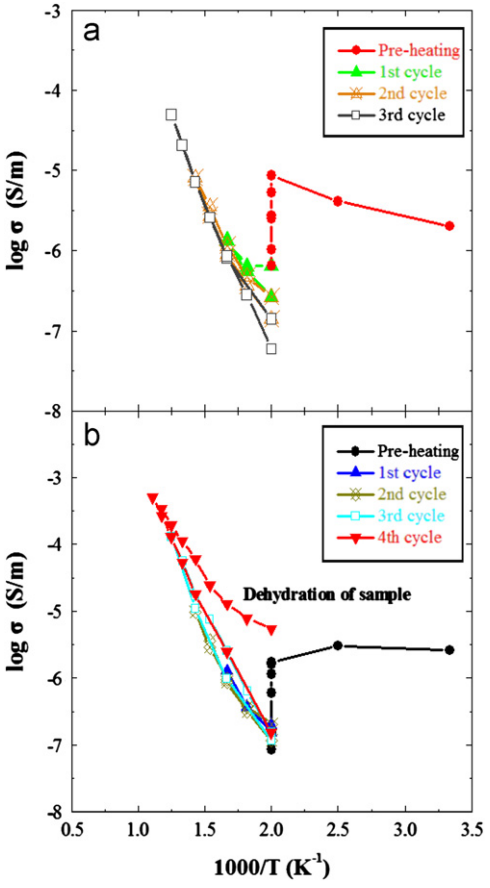

Fig. 3. Typical examples of electrical conductivity measurements for hydrous Al-bearing enstatite as a function of reciprocal temperature. Different symbols indicate the conductivity values for different heating and cooling cycles. (a) Electrical conductivity of aluminous enstatite (run 5K1476). Note that the conductivity values below 800 K are repeatable in 2nd and 3rd cycles. (b) Electrical conductivity of hydrous aluminous enstatite (run 5K1486). Note that the trace of the fourth cooling path is clearly higher than the third cooling and fourth heating paths, suggesting that sample dehydration occurs in the final stage.

examples of electrical conductivity measurements for hydrogen-doped sample are shown in Fig. 3. In run 5K1476 (Fig. 3a), conductivity was measured in three heating-cooling cycles between 500 and 800 K. In general, the conductivity paths become straight and steep by repeating the cycles. On the other hand, a cooling cycle and the next heating cycle show excellent agreement. This reproducibility indicates that conductivities did not suffer from strong oxidation or reduction in the cell as a result of buffering by Mo–MoO_2. The straight line in the third cycle on the Arrhenius plot suggests that adhesive water have completely purged in this cycle. The FT-IR spectroscopy reveals that the water content did not change before and after the conductivity measurement (Fig. 4a and Table 1), suggesting that the structural water was held in enstatite crystals during conductivity measurement.

In run 5K1486 (Fig. 3b), the conductivity values followed the same path by repeating heating and cooling between 500 and 900 K. However, once the sample was heated to 900 K, the conductivity did not decrease significantly with decreasing temperature in the fourth cooling path: the conductivity showed much smaller temperature dependence than before. After conductivity measurement, the FT-IR spectroscopy of recovered samples indicated that the water content in enstatite crystal

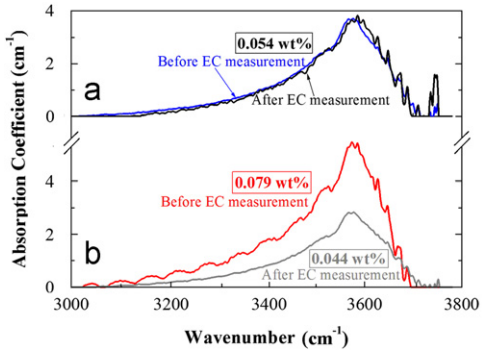

Fig. 4. Representative unpolarized FT-IR spectra of hydrous Al-bearing enstatite before and after the electrical conductivity measurements: (a) 5K1476, no change in water content; (b) 5K1486, loss of water because of dehydration.

was lower (44% lost) than that before the measurement (see Fig. 4b). This observation suggests that dehydration of samples occurred during conductivity measurement. If dehydration occurred, the released high-pressure aqueous fluid is likely to interconnect along grain boundaries (Yoshino et al., 2007), which would mask conductivity of the grain interior, and eventually lead to the apparently high conductivity even though the amount of

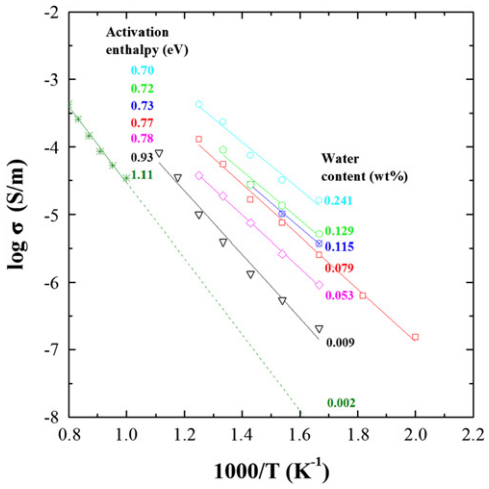

Fig. 5. Proton conduction of aluminous enstatite with various amounts of water (in wt%).

free-water is very small (Yoshino et al., 2006, 2009). Conductivity of hydrogen-doped orthopyroxene cannot be measured at temperature above 900 K, as that of olivine cannot be above 1000 K (Yoshino et al., 2009).

A variation of the absolute conductivity values for both hydrogen-doped and -undoped samples in the temperature range of 500–900 K shows a systematic increase with water content (Fig. 5 and also see Fig. S1 in the supplementary material). Pre-exponential factor (σ_0) and activation enthalpy (H) in Eq. (1) for each sample are summarized in Table 1. Below 900 K, activation enthalpy of hydrogen-doped sample is around 0.9 eV. On the other hand, at higher temperatures than 1300 K, activation enthalpy for the nominally "dry" samples (1K1520) is 1.9 eV.

As shown in Fig. 5, in the temperature range of 500–900 K, conductivity increases by about 3.5 orders of magnitude with increasing water content from 0.002 to 0.241 wt% while the activation enthalpy for proton conduction decreases from 1.11 to 0.70 eV. These observations suggest that proton conduction is the dominant conduction mechanism in the hydrogen-doped enstatite. On the other hand, no clear relationship between the conductivity data and Al concentration was found for hydrous enstatite in this study. This observation implies that proton conduction in enstatite is insensitive to Al_2O_3 content.

4. Discussion

4.1. Charge transport mechanisms in aluminous enstatite

The present study demonstrates that the electrical conductivity of hydrous enstatite largely increases with increasing water content at low temperatures (below 900 K) (Fig. 5). Combining data of hydrogen-undoped and -doped samples, two conduction mechanisms can be identified. The electrical conductivity of hydrous iron-bearing silicate minerals can be expressed by considering the sum of contributions from two conduction mechanisms: hopping (small polaron) and proton conductions.

In the higher temperature range (> 1300 K), small polaron (electron-hole hopping between Fe^{2+} and Fe^{3+} ions) can be considered as a dominant charge carrier. The activation enthalpy (1.9 eV) determined by Eq. (1) falls in a range of small polaron conduction observed in orthoenstatite (Duba et al., 1973; Xu and Shankland, 1999; Dai and Karato, 2009), olivine (Xu et al., 1998, 2000; Yoshino et al., 2006, 2009) and its high-pressure polymorphs (Yoshino et al., 2008a).

The increase of absolute conductivity and decrease of activation enthalpy with increasing water content found in the lower temperature range (Fig. 5 and Table 1) are similar to previous observations for the case of olivine, wadsleyite and ringwoodite (Yoshino et al., 2008a, 2009; Poe et al., 2010). As hydrogen content increases systematically, a decrease of distance to the nearest proton would be a cause of decreasing the activation enthalpy. In this case the activation enthalpy of proton conduction can be described by Eq. (2) in Yoshino et al. (2008a). The results (shown in Fig. S2 in the supplementary material) indicate a fit to this model. The data points obtained from samples with different Al contents were consistently fitted to the same curve, suggesting that the Al content does not have any influence on the proton conduction.

Taking both small polaron and proton conductions into account, the electrical conductivity of hydrous enstatite can be expressed as:

$$\sigma = \sigma_{0h}\exp\left(-\frac{H_h}{kT}\right) + \sigma_{0P}C_W\exp\left(-\frac{H_P^0 - \alpha C_W^{1/3}}{kT}\right) \quad (2)$$

where σ_0 and H are the pre-exponential factor and activation enthalpy, subscripts h and p represent hopping (small polaron) and proton conduction mechanisms, respectively; C_W is water content in weight percent, α is a geometrical factor, and H_P^0 is the activation enthalpy observed at very low water content. The samples with different Al contents were simultaneously fitted by Eq. (2) and the fitting parameters yielding: $\log\sigma_{0h}=3.99(23)$ (S/m), $H_h=1.88(7)$ (eV), $\log\sigma_{0P}=2.58(14)$ (S/m), $H_P^0=0.84(3)$ (eV) and $\alpha=0.08(3)$. The fitting results of electrical conductivities of enstatite as a function of water content are shown in Fig. 6.

Mierdel et al. (2007) proposed that both Al^{3+} and H^+ ions can simultaneously enter into the aluminous enstatite crystal structure by the coupled substitution of $Al^{3+}+H^+$ for Si^{4+} and by the substitution of $Al^{3+}+H^+$ for $2Mg^{2+}$. However, migration of interstitial proton is not accompanied by that of Al^{3+}, and is much faster than that of Al^{3+} ion because of the very small ionic radius of proton. Therefore, the electrical conductivity of hydrous aluminous enstatite strongly depends on hydrogen concentration alone, and is likely to be independent of Al content (Figs. 5 and 6). The trends predicted from Eq. (2) without considering the effect of Al are consistent with those experimentally observed correlations between electrical conductivity and water content (Fig. 6).

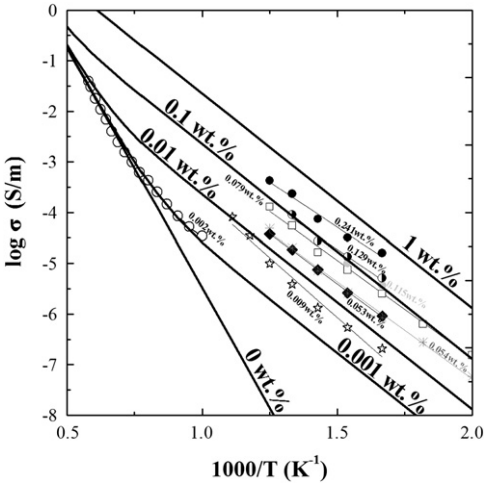

Fig. 6. Calculated electrical conductivity of aluminous enstatite as a function of reciprocal temperature for various water contents. The solid thick lines in the graph indicate the fitting results obtained from Eq. (2) for hydrous Al-bearing enstatite and the numbers represent the water content (in wt%). The symbols denote raw data for each sample with different water contents.

For hydrogen-doped samples, the electrical conductivity measure ments were performed across the phase boundary between orthoenstatite and $P2_1/c$ clinoenstatite. After the conductivity measurement, X-ray diffraction analysis showed that a part of some sample was transformed to $P2_1/c$ clinoenstatite. The maximum temperature for our conductivity measurement of hydrogen-doped samples was located in the stability field of orthoenstatite, whereas the minimum temperature (500 K) was located in that of $P2_1/c$ clinoenstatite. However, in the Arrhenius plot, we did not find any discontinuity across the phase boundary. This implies that the effect of water on the electrical conductivity is almost identical between orthoenstatite and $P2_1/c$ clinoenstatite or small amount of $P2_1/c$ clinoenstatite does not contribute to the bulk conductivity.

4.2. Comparison with previous studies

Fig. 7 shows a comparison of present results on the small polaron conduction of enstatite with some previous studies. Duba et al. (1973) reported that the electrical conductivity of orthopyroxene has a large hysteresis under ambient pressure because of the influence of non-equilibrium processes such as phase transformation from orthoenstatite to protoenstatite. Huebner et al. (1979) investigated the effect of trivalent cations (Al^{3+} or Cr^{3+}) on the electrical conductivity of orthoenstatite at atmospheric pressure. Their results showed that the absolute conductivity increases with Al_2O_3 content. Conductivities of nominally "dry" sample are equivalent to their data, but the temperature dependence (activation energies) in the present study is distinctly larger than these two previous studies: this study, 1.9 eV; Duba et al. (1973); 1.54–1.79 eV, Huebner et al. (1979); 0.92–1.13 eV. The lower activation enthalpies of Huebner et al. (1979) could be attributed to their high Fe/(Mg+Fe) ratio [Mg♯=83], because iron-bearing minerals with higher iron content showed lower activation enthalpy (e.g., garnet: Romano et al., 2006; ringwoodite: Yoshino and Katsura, 2009a; ferropericalse: Yoshino et al., 2011). Otherwise, slightly higher activation enthalpy obtained from this study may imply that ionic conduction due to migration of metal vacancy partially contribute to the bulk conductivity in this temperature range.

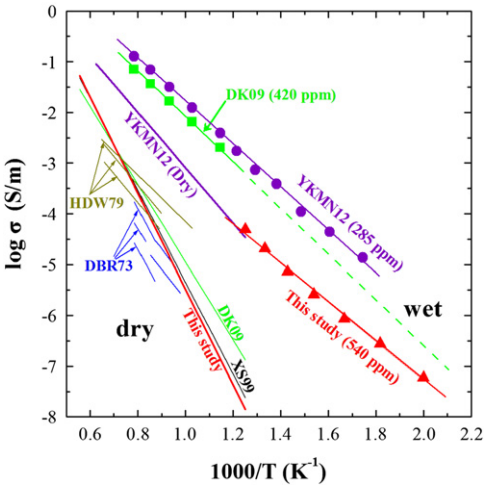

Fig. 7. Comparison of results for the electrical conductivity of orthoenstatite under dry (*solid lines*) and wet (*dashed lines*) conditions. All hydrous samples are assumed to have the same water content (0.05 wt%). *DBR73*—Duba et al. (1973) measured at ambient pressure; *HDW79*—Huebner et al. (1979) measured at ambient pressure; *XS99*—Xu and Shankland (1999) measured at 5 GPa; *DK09*—Dai and Karato (2009) measured mean value for three axes at 8 GPa; *YKMN11*—Yang et al. (2012a) measured at 1.2 GPa.

Xu and Shankland (1999) reported the electrical conductivity of orthoenstatite with 2.89 wt% Al_2O_3 at 5 GPa and at high temperatures ranging from 1273 to 1673 K. Their obtained activation enthalpy of 1.8 eV for hopping conduction is comparable to ours (1.9 eV). Dai and Karato (2009) measured the electrical conductivity of single crystal orthoenstatite with 0.4–0.8 wt% Al_2O_3 at 8 GPa and temperature up to 1473 K. They gave similar conductivity values but lower activation energy of 1.52 eV. As discussed above, this discrepancy in activation energy is mainly due to higher iron content in their samples (Mg♯=82) compared to ours (Mg♯=90). Although the activation enthalpy for proton conduction determined from sample with 0.054 wt% water in this study is consistent with that reported by Dai and Karato (2009), however, proton conduction obtained by Dai and Karato (2009) for single crystal sample with 0.042 wt% water is one order higher than ours (Fig. 7). One possible reason for their high values is that their conductivity measurements were conducted in a stability field of high-pressure ($C2/c$) clinoenstatite (Ulmer and Stalder, 2001; Akashi et al., 2009). Another possible explanation for this discrepancy is the difference of temperature range: the maximum temperature for hydrous samples in this study is 900 K, whereas that in Dai and Karato's (2009) study is 1273 K. Judging from our observation of dehydration at 900 K (Fig. 3b), the enstatite samples of Dai and Karato (2009) were probably dehydrated at a certain temperature above 900 K. Before dehydration, the impedance spectra are characterized by a semicircular shape, suggesting that the equivalent circuit is a single R–C parallel circuit (Fig. 2a). Once the dehydration occurred, the released ionic fluid can be interconnected on the grain boundaries at high temperatures, which caused a distorted and asymmetrical arc or presence of the second arc. Such apparent features imply that the equivalent circuit was not a single R–C parallel circuit and other contributions/mechanisms to the circuit must have existed (Yoshino et al., 2006, 2009; Guo et al., 2011; Yoshino and Katsura, 2012). In fact, a comparison of obtained impedance spectra between ours (Fig. 2a) and figure 2 of Dai and Karato (2009) showed such evidence of dehydration because a significant second arc always appeared in their experiment.

Recently, Yang et al. (2012a) reported the electrical conductivity of enstatite at 0.6–1.2 GPa and up to 1273 K using piston cylinder apparatus. The activation enthalpy for hopping conduction (1.09 eV) is considerably lower than ours and the conductivity values were one to two orders of magnitude higher than the present results. Their results are also significantly higher than the other previous studies (Duba et al., 1973; Huebner et al., 1979; Xu and Shankland, 1999; Dai and Karato, 2009) (Fig. 7). In addition, our dataset indicated that the activation enthalpy of hydrous enstatite decreased with increasing water content, in contrast to the independence of activation enthalpy with water content reported by Yang et al. (2012a). For hopping conduction, these discrepancies could be attributed to a large difference of total Fe content between their ($Fe_{total}O$= ~20.6 wt%, Mg♯=67) and our ($Fe_{total}O$=6~7 wt%, Mg♯=90) studies because the electrical conductivity of the iron-bearing minerals increased with total iron content along the oxygen buffer (Romano et al., 2006; Yoshino and Katsura, 2009a; Yoshino et al., 2011). The other significant difference is oxygen buffer: oxygen fugacity under Mo–MoO_2 buffer (~IW buffer) used in the present study was lower several orders than that under Ni–NiO buffer (~QFM buffer) (Yang et al., 2012a). The electrical conductivity increases with increasing oxygen fugacity which yields a dependence of σ vs. $(fO_2)^{1/6 \text{ or } 2/11}$ (Schock et al., 1989; Du Frane et al., 2005). At the same water content (285 ppmw), the difference for proton conduction is nearly two orders of magnitude (Fig. 7). Furthermore, recent studies (Guo et al., 2011; Dai et al., 2012) have shown that at the same conditions (i.e., T, P, C_{OH}) the electrical conductivity

under Ni–NiO buffer is slightly higher than that under Mo–MoO_2 one, but this effect is very limited (only 0.2 log units difference). Thus, it is difficult to explain this inconsistency by means of the oxygen fugacity.

This difference can be also due to the technical problems. Yang et al. (2012a) used a BN capsule in a platinum capsule whose one end is closed and the other is open. BN capsule can keep a fluid phase to some degree even at high temperatures (Fuji-ta et al., 2011). Moreover, the use of Pt capsule should have prevented escape of fluid phase in the sample. These circumstances lead to the idea that their "high conductivity" is caused by the presence of fluid phase. In order to clarify their technical problems, we performed a series of experiments in which a BN+Pt composite capsule was embedded in our standard assembly (see Appendix A in the supplementary material). Although we were not able to reproduce their results, we have at least found that the combination of BN+Pt composite capsule gives anomalously high conductivity values after heating at 750 K. We also note that the experimental results below 750 K were consistent with those obtained using our standard cell design. Note that the assemblies adopted by the present study are quite permeable, and we purged water at 500 K before conductivity measurement. We have already examined that the presence of adhesive water in the cell assembly could cause high conductivity (Yoshino et al., 2006, 2009; Yoshino and Katsura, 2009b, 2012; Fuji-ta et al., 2011).

4.3. Comparison of conductivity of orthoenstatite and olivine

Fig. 8 shows comparison of electrical conductivities of olivine and enstatite with various water contents. Although there are many studies on conductivity of olivine, our results can be directly compared with those of olivine aggregates of Yoshino et al. (2009) because of use of the same methodology. At lower temperatures (<900 K), hydration greatly enhances the conductivity of aluminous enstatite as well as that of olivine. Proton conduction in aluminous enstatite increases by 1.1 order of magnitude with increasing water content by one order of magnitude. On the other hand, the absolute values of proton conduction in enstatite are by 1.3 order of magnitude larger than those of olivine at the same water content and temperature. The activation enthalpy for proton conduction in enstatite is slightly smaller than that of olivine. For example, the activation enthalpies for

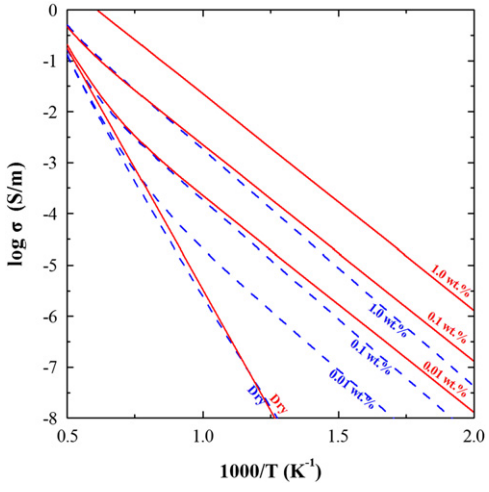

Fig. 8. Comparison of electrical conductivity of Al-bearing enstatite (the red lines from this study) with those of olivine (the blue lines from Yoshino et al., 2009). The numbers denote the water content (in wt%). (For interpretation of the references to color in this figure legend, the reader is referred to the web version of this article.)

enstatite and olivine are 0.84 and 0.92 eV, respectively, at 0.01 wt% H_2O. The activation enthalpy for dry enstatite (1.9 eV) is slightly higher than that for olivine (1.47–1.77 eV). Absolute conductivity values for dry Al-free enstatite are very close to that of olivine at temperatures corresponding to asthenosphere. Thus the prominent difference of conductivity between enstatite and olivine is the absolute magnitude of proton conduction at the same water content.

Electrical conductivity is governed by concentration, mobility and type of point defects in the crystals. Hydrogen in nominally anhydrous minerals can have various speciations (i.e., $H_i^{\bullet}$, H'_{Me} and $(2H)^{X}_{Me}$), where different species could have different mobility (Karato, 2006). Amongst these defect species, free proton $H_i^{\bullet}$ is much more important one especially for electrical conductivity because of its high mobility. If the mobility of free proton is much faster than that of a more abundant defect ($(2H)^{X}_{Me}$), then the electrical conductivity would be controlled by only interstitial proton migration. Consequently, proton conduction should strongly depend on the concentration and mobility of free proton. Recently, deuterium–hydrogen (D–H) exchange experiments in enstatite (Stalder and Behrens, 2006) indicated that hydrogen mobility in orthoenstatite at temperature corresponding to the upper mantle is higher than those in olivine and Ca-rich clinopyroxene. Du Frane and Tyburczy (2012) studied on D–H interdiffusion in hydrous olivine single crystal, their data suggested that all or most of proton contributes to the electrical conductivity for nominally anhydrous minerals. Based on these experimental investigations, the difference in observed conductivities (see Fig. 8) might be caused by the different mobility of hydrogen between orthoenstatite and olivine. However, further studies either experimental measurements or theoretical considerations are required.

4.4. Implications for the conductivity–depth profiles in the upper mantle

In order to assess the presence and distribution of water in the upper mantle, we construct a laboratory-based conductivity–depth profile by extrapolating the present experimental data to the upper mantle in terms of temperature and water content, and compare it with the geophysically observed models. To evaluate the upper bound of contribution of aluminous enstatite to the upper mantle conductivity, the upper mantle is simplified to comprise 40 vol% of aluminous enstatite and 60 vol% of olivine (for details see Appendix B in supplementary information). The effective medium model (Landauer, 1952) was used to calculate the conductivities of two coexisting phases. This model should give the most appropriate average for the electrical conductivity, because the effective medium model yields the average of Hashin–Shtrikman bounds for macroscopically homogeneous and isotropic multiphase materials (Hashin and Shtrikman, 1962; Xu et al., 2000). The geotherm in the deep regions was considered to be adiabatic, which was taken from Katsura et al. (2010). The oxygen fugacity of the upper mantle is assumed to be that of Mo–MoO_2 buffer, which is close to the iron-wüstite (IW) buffer (Xu et al., 1998). Effects of pressure, grain size and additional phases on the bulk rock conductivity are ignored to simplify the model.

Fig. 9 illustrates conductivity–depth profiles for oceanic upper mantle based on the present laboratory data and the above simplifications. As the water content in aluminous enstatite increases from 0.01 to 1.0 wt%, the conductivity values increase by 0.35 log unit. Similar to the case of olivine (Yoshino et al., 2009), if the water content in aluminous enstatite is less than 0.01 wt%, the contribution of proton conduction to the bulk conductivity becomes negligibly small. In the shallow part of

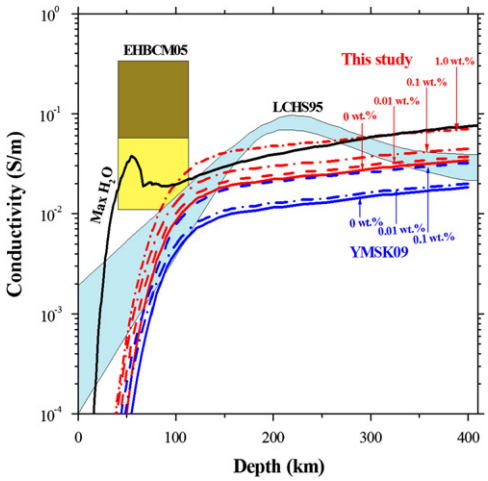

Fig. 9. Laboratory-based conductivity-depth profiles as a function of water contents compared with the previously geophysical models in the upper mantle beneath the Pacific. The *thick black line* indicates the upper bound of the electrical conductivity of the hydrous Al-bearing enstatite. This study (*red lines*) denotes the laboratory-based conductivity-depth profiles with and without water, calculated from the present data for Al-bearing enstatite and Yoshino et al. (2009) for olivine using the effective medium model (Landauer, 1952). YMSK09 (Yoshino et al., 2009), the *blue lines* represent the laboratory-based conductivity–depth profiles derived from the conductivity data of olivine aggregates without considering the contribution of Al-bearing enstatite. The numbers denote the water content (in wt%). Geophysically observed models: LCHS95 (Lizzarralde et al., 1995), EHBCM05 (Evans et al., 2005). (For interpretation of the references to color in this figure legend, the reader is referred to the web version of this article.)

the upper mantle, the conductivity is strongly controlled by the thermal structure of the mantle. Considering a change from conductive to adiabatic at depths around 60 km for oceanic mantle, the increasing rates of conductivity values with depth considerably decrease at that depth. In addition, the upper limit (black line in Fig. 9, details given in Appendix B) of the electrical conductivity for hydrogen-doped aluminous enstatite down to a depth of 410 km was calculated based on pressure dependence of the maximum water solubility in orthoenstatite (Mierdel et al., 2007). Consequently, a sharp increase with depth and the conductivity peak (3.8×10^{-2} S/m) appears around 60 km, but then it distinctly decreases due to the significant drop of the solubility, because the maximum water solubility depends on Al content. Al content in enstatite decreases in this pressure range due to stabilization of garnet. At pressure corresponding to a depth of 100 km, the upper bound of electrical conductivity slightly increases again with depth, because the water solubility in aluminous enstatite increases again as pressure increases (Mierdel et al., 2007). On the other hand, comparing our conductivity–depth profile to olivine one (Yoshino et al., 2009), it is found that the variation is similar to each other, but conductivity values of pure olivine model (Yoshino et al., 2009) yield by 0.4 order of magnitude lower than that of the present olivine+opx model. This is because the electrical conductivity of hydrous aluminous enstatite is 1.3 orders of magnitude higher than that of hydrous olivine assuming that olivine and enstatite contain the same water content.

A comparison of the laboratory-based conductivity–depth profiles estimated in this study with two geophysical models based on magnetotelluric observations beneath the Pacific (Lizzarralde et al., 1995; Evans et al., 2005) is shown in Fig. 9. These models reveal higher conductivity values (order $\sim10^{-1}$ S/m) at the top of the asthenosphere (depth $\sim$60 km, Evans et al., 2005) and at the depth of 200–250 km (Lizzarralde et al., 1995). As illustrated in Fig. 9, although the upper limit of the electrical conductivity of the hydrous aluminous enstatite shows a sharp peak at the depth of 60 km, the conductivity values of our model are at least by 0.6 log unit lower than the high conductivity values (10^{-1} S/m) observed at the Eastern Pacific Rise (Evans et al., 2005).

As shown in Fig. 9, it is found that hydrous aluminous enstatite cannot explain the high-conductivity anomaly observed at the top of the asthenosphere because of the following reasons. First, the water solubility in aluminous enstatite significantly decreases at pressures more than 3 GPa (Mierdel et al., 2007), and therefore the electrical conductivity should once decrease at the depth of 100 km (Fig. 9). To interpret the conductivity of 0.1 S/m (Lizzarralde et al., 1995; Evans et al., 2005), the water content of 6.0 wt% exceeding the maximum solubility of water in aluminous enstatite is required (Mierdel et al., 2007). Second, the proportions of aluminous enstatite in the upper mantle may be low. In order to evaluate the upper bound of contribution of aluminous enstatite to the upper mantle conductivity, we assumed that volume proportion of aluminous enstatite is 40 vol%. Some mantle xenoliths derived from Archean cratons contain numerous orthopyroxene-rich rocks, such as harzburgite, which are expected to exist in the upper mantle (Jordan, 1979). However, the high-pressure phase-equilibrium studies (Takahashi and Ito, 1987; Irifune and Ringwood, 1993; Ulmer and Stalder, 2001) have shown that the amount of orthoenstatite should be small (less than 25 vol%), and decreases with increasing depth in a primitive mantle composition. Such a small volume fraction of enstatite is unlikely to be well-interconnected in the olivine-rich matrix (Yoshino et al., 2008b). Thus, the contribution of hydrous enstatite to the electrical structure in the upper mantle would be limited. The partition coefficient of water of Ca-rich clinopyroxene to olivine is higher than that of Ca-free orthopyroxene to olivine (Grant et al., 2007), and therefore proton conduction of Ca-rich clinopyroxene might influence on the upper mantle conductivity more than that of orthoenstatite. Although Yang et al. (2011) reported the electrical conductivity of hydrous clinopyroxene, their data on hopping and proton conductions (for clinopyroxene as well as orthopyroxene) are always several orders of magnitude higher than other reports because of the methodological problems (see Supplementary information). Therefore, the effect of water on conductivity of Ca-rich clinopyroxene is still in debate. However, further studies, which could help to clarify this controversy and to account for the contribution of hydrous Ca-rich clinopyroxene to the bulk conductivity in the upper mantle, are required in future.

5. Conclusion

The effect of water on the electrical conductivity of aluminous enstatite was investigated at 3 GPa and various temperatures by complex impedance spectroscopy. We measured small polaron and proton conductions using hydrogen-undoped and doped samples, respectively. Relatively higher activation enthalpy (1.9 eV) for the dry enstatite suggest that the dominant conduction mechanism at mantle temperatures could be small polarons, such as that observed for anhydrous olivine because proton conduction characterized by relatively low activation enthalpy is masked by small polaron conduction. For hydrogen-doped enstatite, the conductivity values systematically increase with increasing water content, but the activation enthalpy decreases with water content. Such observations imply that proton conduction is the dominant conduction mechanism for hydrous enstatite at lower temperature range. On the other hand, the electrical conductivity of hydrous enstatite is one order of magnitude higher than that of hydrous olivine with the same amount of water, while the electrical conductivity of hydrogen-undoped Al-free enstatite is similar to that of olivine. The contribution of hydrous Al-bearing enstatite to the bulk conductivity is

considerably small. The hydration of aluminous enstatite is not enough to explain the high conductivity anomaly at the top of the asthenosphere. Alternatively, the presence of minor conductive phases, such as volatile-bearing partial melt (Yoshino et al., 2006, 2010, 2012; Gaillard et al., 2008), could be invoked to account for the geophysical observations.

Acknowledgments

We gratefully thank K. Shinoda, S. Yamashita and A. Shimojuku for their assistance in determining water content of samples and especially wish to thank N. Tomioka for providing helpful discussion in XRD data. The authors also thank F. Gaillard and one anonymous reviewer for their constructive comments which improved the manuscript. This experimental work reported in this paper was performed while B.H. Zhang was a Ph.D. candidate at USTC. This work was supported by funds from the NSF of China (No. 40874034), the National High Technology Research and Development Program of China (863 Program)(No. 2012AA061403) and supported by Grant-in-Aids for Scientific Research from the Japanese Society for the Promotion of Science to T. Yoshino (Grant 20340120).

Appendix A. Supporting information

Supplementary data associated with this article can be found in the online version at http://dx.doi.org/10.1016/j.epsl.2012.09.020.

References

Akashi, A., Nishihara, Y., Takahashi, E., Nakajima, Y., Tange, Y., Funakoshi, K., 2009. Orthoenstatite/clinoenstatite phase transformation in $MgSiO_3$ at high-pressure and high-temperature determined by in situ X-ray diffraction: implications for nature of the X discontinuity. J. Geophys. Res. 114, B04206.

Bell, D.R., Rossman, G.R., Maldener, J., Endisch, D., Rauch, F., 2003. Hydroxide in olivine: a quantitative determination of the absolute amount and calibration of the IR spectrum. J. Geophys. Res. 108, 2105.

Bromiley, G.D., Bromiley, F.A., 2006. High-pressure phase transitions and hydrogen incorporation into $MgSiO_3$ enstatite. Am. Mineral. 91, 1094–1101.

Dai, L.D., Karato, S., 2009. Electrical conductivity of orthopyroxene: implications for the water content of the asthenosphere. Proc. Jpn. Acad. Ser. B 85, 466–475.

Dai, L.D., Li, H.P., Hu, H.Y., Shan, S.M., Jiang, J.J., Hui, K.S., 2012. The effect of chemical composition and oxygen fugacity on the electrical conductivity of dry and hydrous garnet at high temperatures and pressures. Contrib. Mineral. Petrol. 163, 689–700.

Du Frane, W.L., Tyburczy, J.A., 2012. Deutrium–hydrogen exchange in olivine: implications for point defects and electrical conductivity. Geochem. Geophys. Geosys. 13, Q03004.

Du Frane, W.L., Roberts, J.J., Toffelmier, D.A., Tyburczy, J.A., 2005. Anisotropy of electrical conductivity in dry olivine. Geophys. Res. Lett. 32, L24315.

Duba, A., Boland, J.N., Ringwood, A.E., 1973. The electrical conductivity of orthopyroxene. J. Geol. 81, 727–735.

Evans, R.L., Hirth, G., Baba, K., Forsyth, D., Chave, A., Mackie, R., 2005. Geophysical evidence from the MELT area for compositional controls on oceanic plates. Nature 437, 249–252.

Fuji-ta, K., Katsura, T., Ichiki, M., Matsuzaki, T., Kobayashi, T., 2011. Variations in electrical conductivity of rocks above metamorphic conditions. Tectonophysics 504, 116–121.

Gaillard, F., Malki, M., Iacono-Marziano, G., Pichavant, M., Scaillet, B., 2008. Carbonatite melts and electrical conductivity in the asthenosphere. Science 322, 1363–1365.

Guo, X., Yoshino, T., Katayama, I., 2011. Electrical conductivity anisotropy of deformed talc rocks and serpentinites at 3 GPa. Phys. Earth Planet. Inter. 188, 69–81.

Grant, K., Ingrin, J., Lorand, J.P., Dumas, P., 2007. Water partitioning between mantle minerals from peridotite xenoliths. Contrib. Mineral. Petrol. 154, 15–34.

Hashin, Z., Shtrikman, S., 1962. A variational approach to the theory of the effective magnetic permeability of multiphase materials. J. Appl. Phys. 33, 3125–3131.

Huebner, J.S., Duba, A., Wiggins, L.B., 1979. Electrical conductivity of pyroxene which contains trivalent cations: laboratory measurements and the lunar temperature profile. J. Geophys. Res. 84, 4652–4656.

Huebner, J.S., Dillenburg, R.G., 1995. Impedance spectra of hot, dry silicate minerals and rocks, qualitative interpretation of spectra. Am. Mineral. 80, 46–64.

Irifune, T., Ringwood, A.E., 1993. Phase transformations in subducted oceanic crust and buoyancy relationships at depths of 600–800 km in the mantle. Earth Planet. Sci. Lett. 117, 101–110.

Jordan, T.H., 1979. Mineralogies, densities and seismic velocities of garnet lherzolites and their geophysical implications. In: Boyd, F.R., Meyer, H.O.A. (Eds.), The Mantle Sample: Inclusions in Kimberlites and Other Volcanics. AGU, Washington, pp. 1–14.

Karato, S., 1990. The role of hydrogen in the electrical conductivity of the upper mantle. Nature 347, 272–273.

Karato, S., 2006. Influence of hydrogen-related defects on the electrical conductivity and plastic deformation of mantle minerals: a critical review. In: Jacobsen, S.D., van der Lee, S. (Eds.), Earth's Deep Water Cycle, Geophysical Monograph Series, vol. 168. AGU, Washington, D.C, pp. 113–129.

Katsura, T., Yoneda, A., Yamazaki, D., Yoshino, T., Ito, E., 2010. Adiabatic temperature profile in the mantle. Phys. Earth Planet. Inter. 183, 212–218.

Landauer, R., 1952. Electrical resistance of binary metallic mixtures. J. Appl. Phys. 23, 779–784.

Lizzarralde, D., Chave, A.D., Hirth, G., Schultz, A., 1995. Northeastern Pacific mantle conductivity profile from long-period magnetotelluric sounding using Hawaii to California submarine cable data. J. Geophys. Res. 100, 17837–17854.

Mierdel, K., Keppler, H., 2004. The temperature dependence of water solubility in enstatite. Contrib. Mineral. Petrol. 148, 305–311.

Mierdel, K., Keppler, H., Smyth, J.R., Langenhorst, F., 2007. Water solubility in aluminous orthopyroxene and the origin of Earth's asthenosphere. Science 315, 364–368.

Mosenfelder, J.L., Deligne, N.I., Asimov, P.D., Rossman, G.R., 2006. Hydrogen incorporation in olivine from 2–12 GPa. Am. Mineral. 91, 285–294.

Paterson, M.S., 1982. The determination of hydroxyl by infrared absorption in quartz, silicate glasses and similar materials. Bull. Mineral. 105, 20–29.

Poe, B.T., Romano, C., Nestola, F., Smyth, J.R., 2010. Electrical conductivity anisotropy of dry and hydrous olivine at 8 GPa. Phys. Earth Planet. Inter. 181, 103–111.

Romano, C., Poe, B.T., Kreidie, N., McCammon, C.A., 2006. Electrical conductivities of pyrope-almandine garnets up to 19 GPa and 1700 °C. Am. Mineral. 91, 1371–1377.

Schock, R.N., Duba, A.G., Shankland, T.J., 1989. Electrical conduction in olivine. J. Geophys. Res. 94, 5829–5839.

Shankland, T.J., Waff, H.S., 1977. Partial melting and electrical conductivity anomalies in the upper mantle. J. Geophys. Res. 82, 5409–5417.

Stalder, R., Behrens, H., 2006. D/H exchange in pure and Cr-doped enstatite: implications for hydrogen diffusivity. Phys. Chem. Mineral. 33, 601–611.

Takahashi, E., Ito, E., 1987. Mineralogy of mantle periodotite along a model geotherm up to 700 km depth. In: Manghnani, M.H., Shono, Y. (Eds.), High-Pressure Research in Mineral Physics. AGU, Washington, pp. 427–437.

Ulmer, P., Stalder, R., 2001. The $(Mg,Fe)SiO_3$ orthoenstatite–clinoenstatite transitions at high pressures and temperatures determined by Raman-spectroscopy on quenched samples. Am. Mineral. 86, 1267–1274.

Wang, D.J., Mookherjee, M., Xu, Y.S., Karato, S., 2006. The effect of water on the electrical conductivity in olivine. Nature 443, 977–980.

Xu, Y., Poe, B.T., Shankland, T.J., Rubie, D.C., 1998. Electrical conductivity of olivine, wadsleyite and ringwoodite under upper-mantle condition. Science 280, 1415–1418.

Xu, Y., Shankland, T.J., 1999. Electrical conductivity of orthopyroxene and its high pressure phases. Geophys. Res. Lett. 26, 2645–2648.

Xu, Y., Shankland, T.J., Poe, B.T., 2000. Laboratory-based electrical conductivity in the Earth's mantle. J. Geophys. Res. 105, 27865–27875.

Yang, X.Z., 2012. Orientation-related electrical conductivity of hydrous olivine, clinopyroxene and plagioclase and implications for the structure of the lower continental crust and uppermost mantle. Earth Planet. Sci. Lett. 317–318, 241–250.

Yang, X.Z., Keppler, H., McCammon, C., Ni, H.W., Xia, Q.K., Fan, Q.C., 2011. Effect of water on the electrical conductivity of lower crustal clionpyroxene. J. Geophys. Res. 116, B04208.

Yang, X.Z., Keppler, H., McCammon, C., Ni, H.W., 2012a. Electrical conductivity of orthopyroxene and plagioclase in the lower crust. Contrib. Mineral. Petrol. 163, 33–48.

Yang, Y., Xia, Q.K., Feng, M., Liu, S.C., 2012b. OH in natural orthopyroxene: an in situ FTIR investigation at varying temperatures. Phys. Chem. Mineral. 39, 413–418.

Yoshino, T., 2010. Laboratory electrical conductivity measurement of mantle minerals. Surv. Geophys. 31, 163–206.

Yoshino, T., Matsuzaki, T., Yamashita, S., Katsura, T., 2006. Hydrous olivine unable to account for conductivity anomaly at the top of the asthenosphere. Nature 443, 973–976.

Yoshino, T., Nishihara, Y., Karato, S., 2007. Complete wetting of olivine grain boundaries by a hydrous melt near the mantle transition zone. Earth Planet. Sci. Lett. 256, 466–472.

Yoshino, T., Manthilake, G., Matsuzaki, T., Katsura, T., 2008a. Dry mantle transition zone inferred from the conductivity of wadsleyite and ringwoodite. Nature 451, 326–329.

Yoshino, T., Yamazaki, D., Ito, E., Katsura, T., 2008b. No interconnection of ferropericlase in post-spinel phase inferred from conductivity measurement. Geophys. Res. Lett. 35, L22303.

Yoshino, T., Katsura, T., 2009a. Effect of iron content on electrical conductivity of ringwoodite, with implications for electrical structure in the transition zone. Phys. Earth Planet. Inter. 174, 3–9.
Yoshino, T., Katsura, T., 2009b. Reply to comments on ''electrical conductivity of wadsleyite as a function of temperature and water content'' by Manthilake et al.'s discussion. Phys. Earth Planet. Inter. 174, 22–23.
Yoshino, T., Katsura, T., 2012. Re-evaluation of electrical conductivity of anhydrous and hydrous wadsleyite. Earth Planet. Sci. Lett. 337–338, 56–67.
Yoshino, T., Matsuzaki, T., Shatskiy, A., Katsura, T., 2009. The effect of water on the electrical conductivity of olivine aggregates and its implications for the electrical structure of the upper mantle. Earth Planet. Sci. Lett. 288, 291–300.
Yoshino, T., Laumonier, M., Mclsaac, E., Katsura, T., 2010. Electrical conductivity of basaltic and carbonatite melt-bearing peridotites at high pressures: implications for melt distribution and melt fraction in the upper mantle. Earth Planet. Sci. Lett. 295, 593–602.
Yoshino, T., Ito, E., Katsura, T., Yamazaki, D., Shan, S., Guo, X., Nishi, M., Higo, Y., Funakoshi, K., 2011. Effect of iron content on electrical conductivity of ferropericlase with implications for the spin transition pressure. J. Geophys. Res. 116, B04202.
Yoshino, T., Mclsaac, E., Laumonier, M., Katsura, T., 2012. Electrical conductivity of partial molten carbonatite peridotite. Phys. Earth Planet. Inter. 194–195, 1–9.